

A PASSIVE JUMPING MECHANISM

Phanindra Tallapragada *

Dept. of Mechanical Engineering
Clemson University
Clemson, S.C, 29632
Email: ptallap@clemson.edu

Jake Buzhardt

Dept. of Mechanical Engineering
Clemson University
Clemson, S.C, 29632
Email: jbzhar@g.clemson.edu

Robert Seney

Dept. of Mechanical Engineering
Clemson University
Clemson, S.C, 29632
Email: rseney@g.clemson.edu

ABSTRACT

In this paper we present a novel unactuated mechanism that utilizes gravity to jump. The passive jumper is a hoop whose center of mass does not coincide with its geometric center. When the hoop rolls down an inclined plane, the center of mass of the hoop moves along a cycloid. As the hoop gains speed moving down the inclined plane, the normal reaction between the hoop and the plane becomes insufficient to ensure contact between the hoop and the plane. This allows the hoop to ‘jump’. Experiments and analysis show that such a jump can be significant, with the jump height from the plane being as high as one body length (diameter) of the hoop. The mechanics of the passive jumping hoop powered by gravity investigated in this paper can inspire the design of actuated jumping robots that can both roll and jump.

1 Introduction

The ability of a robot to hop or jump even by a small height can add versatility to its locomotion and enable it to move on terrain that it otherwise may have difficulty doing so. Even robots in structured environments will benefit from an ability to hop on small steps or jump over obstacles. For robots that are small in size, jumping also offers improvement in locomotion efficiency. Several designs of robots have sought to incorporate the jumping or hopping gait in the repertoire of a robot’s gaits. The common feature of the designs that produce jumping, are a mechanism to store potential energy that can be released in a short interval. The resulting conversion of the potential energy to kinetic energy in

the vertical direction leads to a jump. The most popular method to achieve such storage and release of energy is via traditional elastic elements, such as compression or torsional springs or flexural plates and columns. Some well known examples that adopt such design include the MSU jumper [1], the Penn Jerboa [2], the Grillo [3] and the Salto [4] and other impressive bioinspired micro jumping robots [5]. Other means of releasing stored energy have been explored. For instance the Boston Dynamics sand-flea uses a carbon dioxide powered piston to launch itself to very impressive heights [6].

The present paper takes a radically new approach and instead explores the concept of a passive jumper. Such a concept is inspired by the passive walking legged mechanisms [7–11] that utilize gravity alone to walk down on an inclined plane. We investigate the dynamics of a rolling wheel or a hoop on an inclined plane. The hoop is such that its center of mass is not coincident with the geometric center of the hoop. As the hoop rolls down the plane, the eccentric center of mass experiences a centrifugal force directed towards the center of the hoop, which when pointing downwards results in a decrease in the normal reaction force between the hoop and the inclined plane. If the parameters of the system are properly chosen, the normal reaction becomes zero at some time and the hoop ‘jumps’ off the plane. We analyze this phenomenon and present experimental evidence for a passive jumper.

While the passive jumper requires an inclined plane to jump, it is possible to design a rolling jumper that is driven by a motor that mimics the role of the inclined plane. A jumping robot based on a wheel can combine the advantages of wheeled motion with the ability to jump.

*Address all correspondence related to the paper should be addressed to this author.

2 Dynamic model

The mechanical system consists of a thin hoop of mass m and radius R , with its mass uniformly distributed around the circumference of the hoop. A particle of mass m_p is attached to the hoop at a distance of L from the center of the hoop. The hoop is released from rest on an inclined plane with slope angle θ . It is assumed that the friction between the hoop and the inclined plane is sufficient to prevent slipping. A schematic of the hoop and inclined plane system is shown in Fig. 1 with the generalized coordinates x , y , and ϕ denoted.

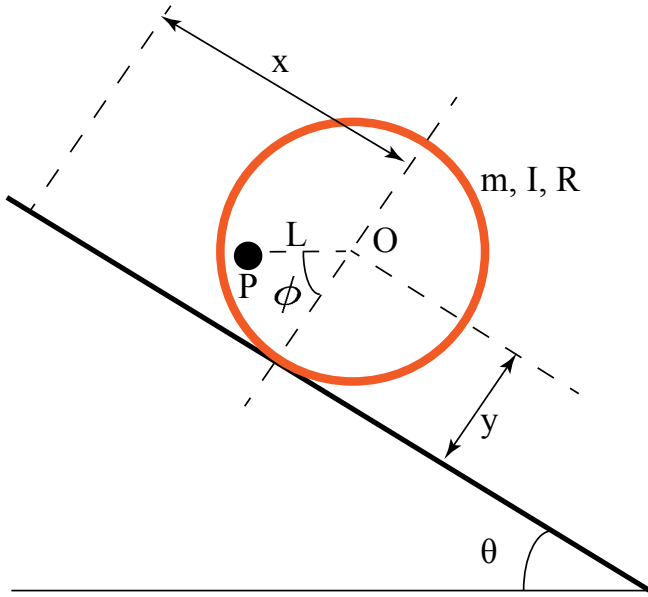


Figure 1: Schematic of the system of a hoop of mass m , moment of inertia I , and radius R with an offset point mass m_p rolling on a plane inclined at an angle θ . The generalized coordinates x, y, ϕ are also depicted here.

The center of the hoop denoted by O has coordinates (x, y) and the center of mass of the hoop is located at a distance of $r = \frac{m_p}{m+m_p}L$ from the center O . The point of attachment of the particle of mass m_p is denoted by P . The clockwise angle made by the line OP with respect to a line perpendicular to the plane is denoted by ϕ . The system has two holonomic constraints in pure rolling motion,

$$y - R = 0 \quad (1)$$

and

$$x - R\phi = 0. \quad (2)$$

Assuming that the friction force between the hoop and the plane is high enough to prevent slipping, the configuration space of the system can be parameterized by three generalized coordinates, $q = (x, y, \phi)$. The equations of motion can be derived in a straightforward manner using the Euler-Lagrange equations and the generalized forces required to enforce the constraints (1) and (2) can be obtained using the method of Lagrange multipliers. The kinetic energy of the system is

$$\mathcal{T} = \frac{1}{2}m_p(\dot{x}^2 + \dot{y}^2 + L^2\dot{\phi}^2 - 2\dot{x}\dot{\phi}L\cos\phi + 2\dot{y}\dot{\phi}L\sin\phi) + \frac{1}{2}m(\dot{x}^2 + \dot{y}^2) + \frac{1}{2}I\dot{\phi}^2. \quad (3)$$

The potential energy is defined as

$$\mathcal{V} = (m + m_p)g(y\cos\theta - R\phi\sin\theta) - m_pgL\cos(\theta + \phi). \quad (4)$$

The Lagrangian is

$$\mathcal{L} = \mathcal{T} - \mathcal{V} \quad (5)$$

and the Euler-Lagrange equations, with constraints implemented using the method of Lagrange undetermined multipliers [12, 13] are

$$\frac{d}{dt} \left(\frac{\partial \mathcal{L}}{\partial \dot{q}_i} \right) - \frac{\partial \mathcal{L}}{\partial q_i} = \lambda_j \frac{\partial f_j}{\partial q_i}. \quad (6)$$

Here the expressions f_j are given by the left hand side of the constraint equations (1) and (2).

Applying Eq. (6), the equations governing the motion of this system are found to be

$$(m + m_p)\ddot{x} - m_p\ddot{\phi}L\cos\phi + m_p\dot{\phi}^2L\sin\phi - (m + m_p)g\sin\theta = \lambda_f \quad (7)$$

$$(m + m_p)\ddot{y} + m_p\ddot{\phi}L\sin\phi + m_p\dot{\phi}^2L\cos\phi + (m + m_p)g\cos\theta = \lambda_n \quad (8)$$

$$(I + m_pL^2)\ddot{\phi} - m_p\dot{x}L\cos\phi + m_o\dot{y}L\sin\phi + m_pgL\sin\theta + \phi = -\lambda_f R \quad (9)$$

where for notational clarity, we let λ_f represent the Lagrange multiplier associated with the friction required to satisfy (2) and let λ_n represent the Lagrange multiplier associated with the normal force required to satisfy (1).

In the following sections, we divide the dynamics of the system into two distinct phases: 1) a pure rolling phase in which the hoop rolls without slip on the plane, with both Eqs (1) and (2) satisfied and 2) a flight phase in which the hoop loses contact with the plane and neither constraint is satisfied. We note here that in certain cases, it may be necessary to consider an intermediate phase, in which the hoop remains in contact with the plane, but may slip. Analytical modeling of such a phase which requires careful consideration of the coefficients of friction is possible, however the experimental verification of such roll-slip transitions are harder to detect. As we will discuss later, neglecting such a roll-slip transition leads to only negligible errors in the analytical solution compared to the experiments.

2.1 Rolling phase of motion

During the pure rolling phase of motion, the constraint equations (2) and (1) must be satisfied, thus they may be used to reduce the system to a single second-order differential equation of ϕ that fully defines the dynamics. This equation is given by

$$\begin{aligned} \left(I + m_p L^2 + (m + m_p) R^2 - 2m_o L R \cos \phi \right) \ddot{\phi} + m_p L \dot{\phi}^2 R \sin \phi \\ = (m + m_p) g R \sin \theta - m_p g L \sin(\theta + \phi) \end{aligned} \quad (10)$$

The generalized forces of constraint are then given as follows. The normal reaction, λ_n between the hoop and the inclined plane is

$$\lambda_n = m_p \ddot{\phi} L \sin \phi + m_p L \dot{\phi}^2 \cos \phi + (m + m_p) g \cos \theta. \quad (11)$$

and the force due to friction between the hoop and the plane is

$$\lambda_f = \left((m + m_p) R - m_p L \cos \phi \right) \ddot{\phi} + m_p L \dot{\phi}^2 \sin \phi - (m + m_p) g \sin \theta. \quad (12)$$

2.2 Flight phase of motion

During the flight phase of the hoop's motion, the constraints given by (1) and (2) are no longer satisfied, and so the governing equations cannot be reduced. Therefore, to fully specify the dynamics, three differential equations are required, and may be found by setting the generalized forces of constraint λ_f and λ_n to zero in Eqs. (7-9). Thus, the equations governing the flight

phase dynamics are given by

$$\begin{aligned} (m + m_p) \ddot{x} - m_p \ddot{\phi} L \cos \phi + m_p \dot{\phi}^2 L \sin \phi - (m + m_p) g \sin \theta &= 0 \\ (m + m_p) \ddot{y} + m_p \ddot{\phi} L \sin \phi + m_p \dot{\phi}^2 L \cos \phi + (m + m_p) g \cos \theta &= 0 \\ (I + m_p L^2) \ddot{\phi} - m_p \ddot{x} L \cos \phi + m_o \ddot{y} L \sin \phi + m_p g L \sin \theta + \phi &= 0 \end{aligned} \quad (13)$$

3 Experimental and Simulation Results

3.1 Experimental Setup

Before examining the results of the numerical simulations of these dynamics, we first discuss the experimental realization of this system. The hoop-mass system was constructed by first 3D-printing a hoop frame with a diameter of 8.2 cm, as shown in Fig. 2. This frame was designed with five circular channels into which steel cylindrical weights would be inserted. The hoop frame was printed in PLA plastic and found to weigh approximately 8.2 grams without the addition of any added masses. After printing the frame of the hoop, five steel weights were inserted into the cylindrical channels to represent the offset point mass, m_p . Each of the masses was found to weigh 5 grams, for a total of 20 grams. Thus, the hoop frame and added mass together weigh approximately 28.2 grams. In all numerical simulations discussed in this paper, these values are used for the mass of the hoop and the point mass, and it is assumed that the point mass lies on the radius of the hoop. That is, in simulation we take $L = R$.

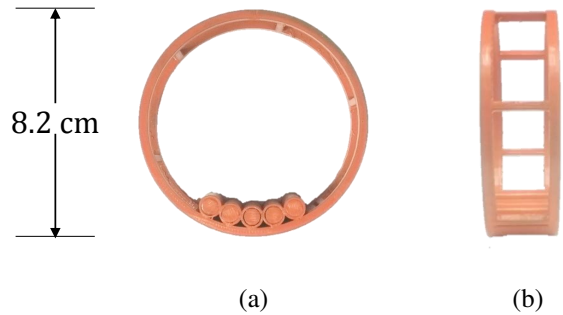


Figure 2: 3D-printed hoop used in experiments.

For the experimental setup, the hoop is placed on a wooden inclined plane with a slope angle of approximately $\theta = 0.40 \text{ rad} = 22.9^\circ$. Videos of the hoop's motion was recorded using a Photron FASTCAM SA4 camera at a frame rate of 1000 frames per second. A transparent tape was stuck along a diameter of the hoop, with one end point at the center of the added mass

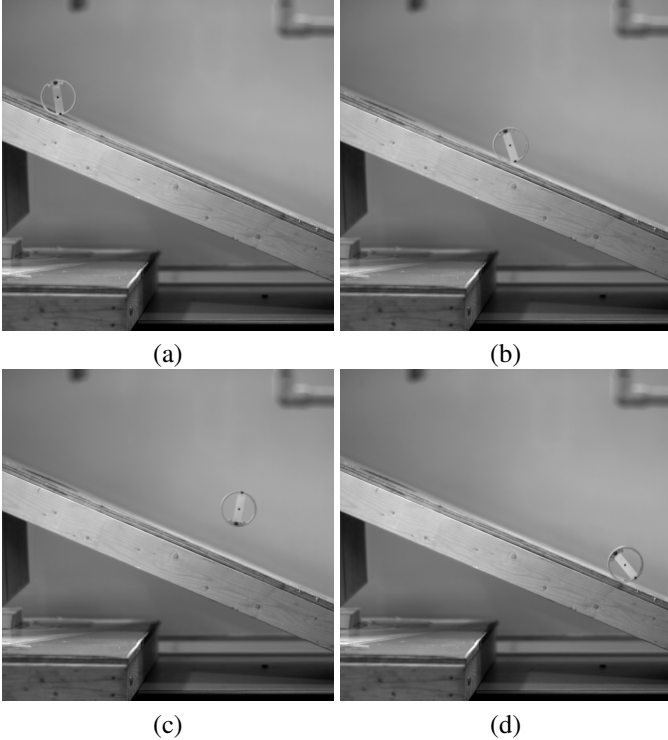


Figure 3: Image data recorded at various instants during the experiment. (a) Image taken after hoop has begun steady rolling motion, but well before losing contact ($t = 0.111$ s in Fig 4). (b) Hoop at the instant before visibly losing contact ($t = 0.330$ s in Fig 4). (c) Hoop at maximum height y , normal to the incline ($\Delta t = 0.129$ s in Fig 6). (d) Hoop at the instant of contacting the incline after the jump ($\Delta t = 0.198$ s in Fig 6).

and the other at a point diametrically opposite to it. Three black markings were placed on this tape: one at the location of the point mass, the second at the diametrically opposite point, and the third at the center of the hoop. These markings were placed in order to enable the points to be easily tracked in the videos and images of the hoop in post-processing. Image data was gathered from the point of release through the jump until just after the collision of the hoop with the inclined plane. This entire interval spanned approximately 0.593 seconds. Select frames from this image data are shown below in Fig. 3.

From the image data collected, the location of the center of the hoop and the location of the point mass were tracked for each instant that a frame was recorded. These frames were recorded at intervals of 0.001 seconds. From this instantaneous position data, the angle ϕ is computed and the velocities are determined using a central-differencing method.

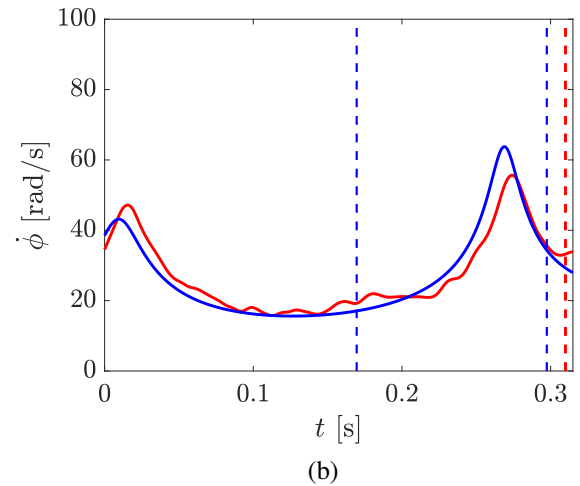
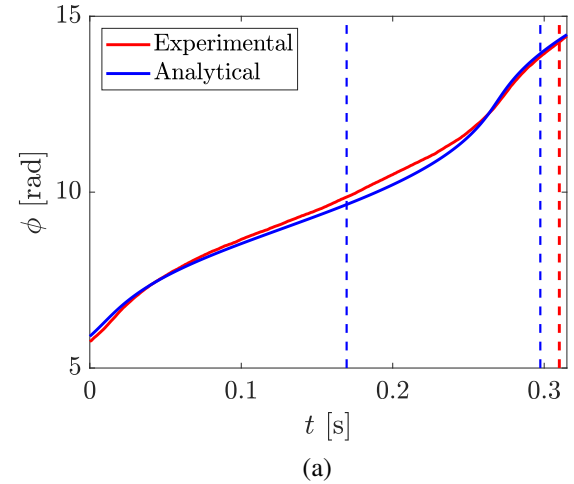


Figure 4: Comparison of experimental measurements of the angle ϕ and $\dot{\phi}$ with predicted values from the analytical model during the rolling phase of the dynamics. Vertical dashed lines indicate when the jump occurs in the experiment and when the normal force is predicted to vanish by the analytical model respectively.

3.2 Rolling phase of motion

In order to compare numerical simulation of the analytical model, the equation (10) governing the rolling motion of the hoop is integrated forward in time using MATLAB's ordinary differential equation solver `ode45`. The initial condition is chosen to coincide with the angle ϕ and angular velocity $\dot{\phi}$ computed from the experimental image data. In this simulation, the normal reaction λ_n required to keep the hoop in contact with the plane and the friction force λ_f required to maintain the rolling motion without slip are computed using equations (11) and (12) respectively. These two parameters may then be used to predict when the hoop will lose contact with the plane ($\lambda_n = 0$) or when the hoop will begin to experience slip.

Numerical values of ϕ and $\dot{\phi}$ found by integrating the analytical model are shown alongside the experimentally measured values in Figs 4 (a) and (b) respectively. In this figure, the instants in time where the analytical model predicts that the normal force will vanish are shown by vertical dashed blue lines. The time instant at which the hoop begins to visibly lose contact with the surface of the inclined plane in the experiment is shown by a vertical dashed red line.

We note that in Fig 4, there are two instances shown at which the normal reaction is predicted to vanish by the analytical model. The second instance is close in time to that of the experimentally realized jump, but the first instance occurs well before the jump. A plot of the constraint forces, the normal reaction and the friction force, calculated from (11)-(12) are shown in Fig. 5 (a) and Fig. 5 (b) respectively. The normal reaction becomes zero at about $t = 0.17$ s, but nevertheless stays close to zero before increasing again to a large value at a later time. The constraint force required to enforce the no-slip condition as shown in Fig. 5 could be more than the friction force which is bounded above by the maximum allowable values of static friction, $\mu_s N$, where μ_s is the coefficient of static friction. As the normal reaction decreases, the friction force converges to zero faster, producing a slip before loss of contact with the plane occurs. Since work is done by the friction force during a slip, it reduces the rate of increase of the kinetic energy of the hoop as it moves down the inclined plane. We hypothesize that this reduction in kinetic energy of the hoop prevents the normal reaction from decreasing to zero. This prevents the hoop from losing contact with the plane.

A transition to slip motion occurs a small time interval before the time the normal reaction becomes zero at about $t = 0.3$ s. This transition is even observable in experiments just prior to the hoop's loss of contact with the plane. Once again we neglect these roll-slip transitions before the jump. In both the cases of the slip dynamics, the slip dynamics persist only for a very small interval of time, less than 0.005s. The effect of ignoring these transitions is that the kinetic energy of the hoop is predicted to be higher than observed in experiment. The increased kinetic energy of the hoop, leads to a jump at an earlier time in the simulation than observed.

3.3 Flight phase of motion

Once the normal reaction which maintains the constraint (1) vanishes, the hoop loses contact with the inclined plane and begins the flight phase of its motion. During this phase, three equations given by (13), are required to fully describe the dynamics. In simulation, these are integrated forward in time from an initial condition based on the end condition of the rolling phase - the point at which the normal force vanishes and the hoop loses contact. If the angle ϕ and angular velocity $\dot{\phi}$ at that instant are denoted ϕ_f and $\dot{\phi}_f$ respectively, then the initial conditions for the

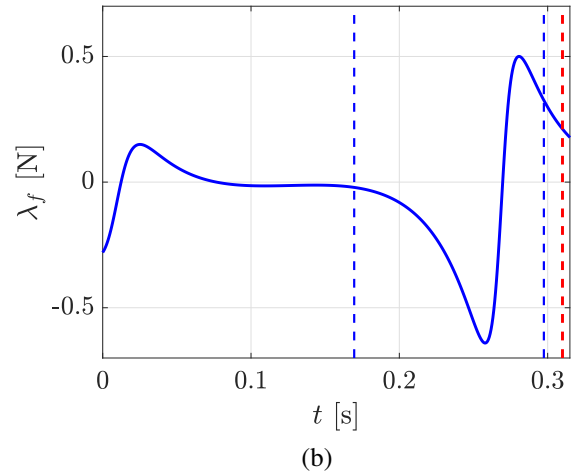
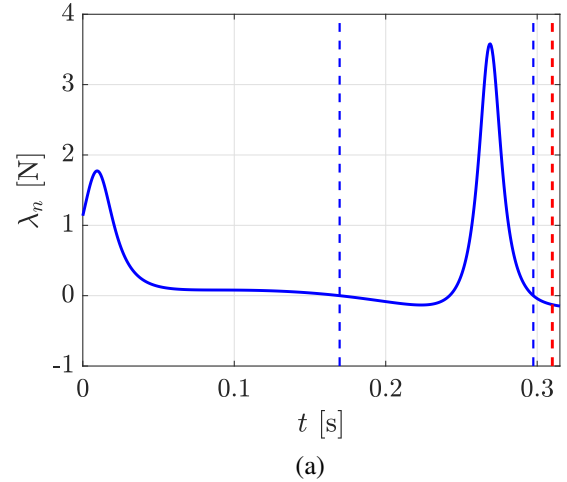


Figure 5: (a) Normal force and (b) friction force required to maintain constraints (1) and (2) respectively during the pure rolling phase of motion.

flight phase of motion, denoted by the subscript i , would be

$$\begin{aligned} x_i &= \phi_f R & \dot{x}_i &= \dot{\phi}_f R \\ y_i &= R & \dot{y}_i &= 0 \\ \phi_i &= \phi_f & \dot{\phi}_i &= \dot{\phi}_f \end{aligned}$$

Since there is a discrepancy (less than 5%) between the simulation and the experimental data with regard to the instant when the jump begins, a small error is introduced in the initial conditions for the flight phase in the simulation, which leads to an over prediction of the jump height. For this reason, a correction to the initial conditions of the flight phase is used based on the experimental data. With this small correction to the initial conditions, the numerical simulation of the flight phase matches

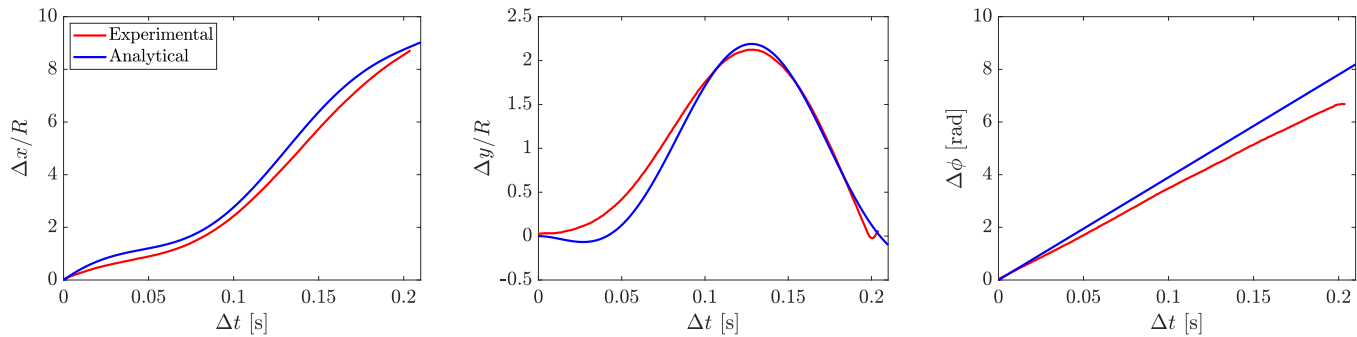


Figure 6: Comparison of experimentally measured values of the generalized coordinates x , y , and ϕ with the values predicted by numerical simulation of the analytical model during the flight phase of motion.

closely with the experimental data, as is shown in Fig. 6. In these figures, the change in each of the generalized coordinates during the flight phase is shown, beginning from the instant at which the hoop loses contact ($\Delta t = 0$ s). The experiments and the simulations reveal that the hoop can jump to a height of one diameter above the plane. This is a remarkable jump for a completely passive mechanism.

Furthermore, we also verify that if the hoop is allowed to jump at the first instance when the normal reaction becomes zero, the height of the jump is negligibly small, less than 0.05 times the diameter, implying that the kinetic energy of the hoop is small at the instant of jump-off. This provides further evidence to support our hypothesis that a small reduction in the kinetic energy due to roll-slip transitions in fact prevents this spurious jump in the experiment.

4 Conclusion

We have shown both analytically and experimentally that a passive jumping mechanism can be constructed from a circular hoop whose center of mass does not coincide with its geometric center. These results show that this simple mechanism can achieve jumps of significant heights, even as much as one body length. Furthermore, we have derived an analytical model from first principles and shown that this model provides a close approximation to the experimentally realized system. Future work will focus on improving the analytical model by including roll-slip-roll and roll-slip-jump transitions as well as achieving multiple jumps. The understanding of the passive dynamics provided by this work can serve as a starting point for the design of versatile robots that have the ability to both roll and jump.

REFERENCES

- [1] J. Zhao, J. Xu, B. Gao, F. Cintron, M. Mutka, and L. Xiao. Msu jumper: A single-motor-actuated miniature steerable

jumping robot. *IEEE Transactions on Robotics*, 29(3):602–614, 2013.

- [2] A. De and D. Koditschek. Parallel composition of templates for tail-energized planar hopping. In *IEEE International Conference on Robotics and Automation*, pages 4562–4569, 2015.
- [3] U. Scarfogliero, C. Stefanini, and P. Dario. Design and development of the long-jumping grillo minirobot. In *IEEE International Conference on Robotics and Automation*, pages 467–472, 2007.
- [4] D. W. Haldane, M. M. Plecnik, J. K. Yim, and R. S. Fearing. Robotic vertical jumping agility via series-elastic power modulation. *Science Robotics*, 1(1), 2008.
- [5] V. Zaytsev, U. Ben Hanan, A. Weiss, G. Ksa, and A. Ayali. A locust-inspired miniature jumping robot. *Bioinspiration and Biomimetics*, 10(6), 2015.
- [6] Boston dynamics sand flea robot demonstrates astonishing jumping skills. *IEEE Spectrum Blog*, 2012.
- [7] T. McGeer. Passive dynamic walking. *International Journal of Robotics Research*, 9(2), 1990.
- [8] A. Goswami, B. Espiau, and A. Keramane. Limit cycles in a passive compass gait biped and passivity-mimicking control laws. *Autonomous Robots*, 4(3):273286, 1997.
- [9] M. Garcia, A. Chatterjee, A. Ruina, and M. Coleman. The simplest walking model: stability, complexity, and scaling. *Journal of Biomechanical Engineering*, 120(2):281–288, 1998.
- [10] S. Collins, A. Ruina, R. Tedrake, and M. Wisse. Efficient bipedal robots based on passive-dynamic walkers. *Science*, 307(5712):1082–1085, 2005.
- [11] J.D. Galloway II C.L. Trevino and P.A. Bhounsule. A three-dimensional printed, nonassembly, passive dynamic walking toy: Design and analysis. *ASME J. Mechanisms Robotics*, 10(6):061009–061009–8, 2018.
- [12] H. Goldstein. *Classical Mechanics*. Addison-Wesley, 1980.
- [13] D. T. Greenwood. *Classical Dynamics*. greenwood, 1997.